Regulation of TRPM2 by Extra- and Intracellular Calcium

John Starkus,[1,2] Andreas Beck,[2] Andrea Fleig,[2] and Reinhold Penner[2]

[1]Pacific Biosciences Research Center, University of Hawaii, Honolulu, HI 96822
[2]Laboratory of Cell and Molecular Signaling, Center for Biomedical Research at The Queen's Medical Center and John A. Burns School of Medicine at the University of Hawaii, Honolulu, HI 96813

TRPM2 is a calcium-permeable nonselective cation channel that is opened by the binding of ADP-ribose (ADPR) to a C-terminal nudix domain. Channel activity is further regulated by several cytosolic factors, including cyclic ADPR (cADPR), nicotinamide adenine dinucleotide phosphate (NAADP), Ca^{2+} and calmodulin (CaM), and adenosine monophosphate (AMP). In addition, intracellular ions typically used in patch-clamp experiments such as Cs^+ or Na^+ can alter ADPR sensitivity and voltage dependence, complicating the evaluation of the roles of the various modulators in a physiological context. We investigated the roles of extra- and intracellular Ca^{2+} as well as CaM as modulators of ADPR-induced TRPM2 currents under more physiological conditions, using K^+-based internal saline in patch-clamp experiments performed on human TRPM2 expressed in HEK293 cells. Our results show that in the absence of Ca^{2+}, both internally and externally, ADPR alone cannot induce cation currents. In the absence of extracellular Ca^{2+}, a minimum of 30 nM internal Ca^{2+} is required to cause partial TRPM2 activation with ADPR. However, 200 μM external Ca^{2+} is as efficient as 1 mM Ca^{2+} in TRPM2 activation, indicating an external Ca^{2+} binding site important for proper channel function. Ca^{2+} facilitates ADPR gating with a half-maximal effective concentration of 50 nM and this is independent of extracellular Ca^{2+}. Furthermore, TRPM2 currents inactivate if intracellular Ca^{2+} levels fall below 100 nM irrespective of extracellular Ca^{2+}. The facilitatory effect of intracellular Ca^{2+} is not mimicked by Mg^{2+}, Ba^{2+}, or Zn^{2+}. Only Sr^{2+} facilitates TRPM2 as effectively as Ca^{2+}, but this is due to Sr^{2+}-induced Ca^{2+} release from internal stores rather than a direct effect of Sr^{2+} itself. Together, these data demonstrate that cytosolic Ca^{2+} regulates TRPM2 channel activation. Its facilitatory action likely occurs via CaM, since the addition of 100 μM CaM to the patch pipette significantly enhances ADPR-induced TRPM2 currents at fixed $[Ca^{2+}]_i$ and this can be counteracted by calmidazolium. We conclude that ADPR is responsible for TRPM2 gating and Ca^{2+} facilitates activation via calmodulin.

INTRODUCTION

TRPM2 is a widely expressed plasma membrane protein with dual function as ion channel and ADP-ribose (ADPR)–specific pyrophosphatase (Perraud et al., 2001; Sano et al., 2001; Hara et al., 2002; Fleig and Penner, 2004; Harteneck, 2005; Scharenberg, 2005). Binding of ADPR has been proposed to be the primary gating mechanism of TRPM2 (Perraud et al., 2001; Kolisek et al., 2005). In addition, TRPM2 currents can be activated by oxidative stress inducers independently of pyrophosphatase activity (Herson and Ashford, 1997; Hara et al., 2002; Wehage et al., 2002) and by high concentrations of cyclic ADPR (cADPR) or nicotinamide adenine dinucleotide phosphate (NAADP) (Kolisek et al., 2005; Beck et al., 2006). ADPR and cADPR synergize to efficiently activate TRPM2 currents at ADPR levels in the low nanomolar range (Kolisek et al., 2005), but only in K^+-based and not Cs^+-based solutions (Beck et al., 2006; Heiner et al., 2006). TRPM2 supports Na^+ and Ca^{2+} influx, thereby modulating membrane potential as well as intracellular Ca^{2+} levels (Perraud et al., 2001; Sano et al., 2001; Hara et al., 2002; McHugh et al., 2003). The channel's sensitivity to ADPR is also facilitated by intracellular Ca^{2+} (Herson et al., 1997; Perraud et al., 2001; McHugh et al., 2003; Heiner et al., 2006), which acts as a positive feedback mechanism on channel activity. The facilitatory action of Ca^{2+} could be due to a direct Ca^{2+}-binding site on the channel or conferred by an endogenous Ca^{2+} sensor such as calmodulin. Recently, calmodulin binding to the channel's N terminus has been implicated to confer TRPM2's calcium sensitivity as demonstrated by Mn^{2+} quenching using FuraRed fluorescent measurements while co-overexpressing various calmodulin mutants (Tong et al., 2006).

Ca^{2+} dependence of TRPM2 activity has been reported in U937 monocytes (Perraud et al., 2001), Cri-G1 insulinoma cells (Herson and Ashford, 1997; Inamura et al., 2003), Jurkat T cells (Beck et al., 2006), and in HEK293 cells overexpressing transient receptor potential melastatin 2 (TRPM2) (Perraud et al., 2001; McHugh et al., 2003). For human neutrophil granulocytes it has been proposed that resting levels of cytosolic ADPR are sufficient to enable TRPM2 activation by elevation of

Correspondence to Reinhold Penner: rpenner@hawaii.edu

Abbreviations used in this paper: ADPR, ADP-ribose; CaM, calmodulin; IP_3, inositol 1,4,5 trisphosphate; nDVF, nominally divalent-free; NMG, *N*-methyl-D-glucamine; SERCA, sarco/endoplasmatic calcium ATPase; TRPM2, transient receptor potential melastatin 2.

TABLE I

Composition of Intracellular Solutions in mM

	Free Ca	0 Ca	30 nM Ca	100 nM Ca	150 nM Ca	300 nM Ca	500 nM Ca	1000 nM Ca
BAPTA	0	10	10	10	10	10	10	10
$CaCl_2$	0	0		3.1	4	5.7	6.87	8.2
K-glutamate	140	120	120	120	120	120	120	120
NaCl	8	8	8	8	8	8	8	8
$MgCl_2$	1	1	1	1	1	1	1	1
HEPES	10	10	10	10	10	10	10	10

pH 7.2 (adjusted with NaOH or HCl); osmolarity, 300–310 mOsm (adjusted with sucrose). WebMax parameters: temperature = 24°C, pH = 7.2, ionic strength = 0.16.

intracellular Ca^{2+} above basal levels of 100 nM (Heiner et al., 2006), practically obviating ADPR production by a second messenger system. However, aside from the study in Jurkat T cells (Beck et al., 2006), all of the above investigations were conducted in either Cs^+- or Na^+-based intracellular solutions. Our work has shown that the sensitivity of TRPM2 channels to ADPR and cADPR is significantly affected by the primary cation of the internal saline, in that the synergistic effect of cADPR on ADPR-induced gating is only observed in the presence of K^+ but not Cs^+ (Beck et al., 2006). Furthermore, exposure of TRPM2 to high intracellular Na^+ concentrations confers voltage-dependent inactivation at negative potentials that is not seen when using Cs^+ (Herson et al., 1997; Perraud et al., 2001). Neither the characteristics of Ca^{2+} sensitivity nor the kinetic behavior of TRPM2 are known in more physiologically relevant K^+-based intracellular conditions. The aim of this paper was therefore to characterize the role of Ca^{2+} in TRPM2 function using K^+-based intracellular solutions, focusing on channel kinetics, the dependence on the source of Ca^{2+}, and the source of the channel's Ca^{2+} sensitivity itself.

MATERIALS AND METHODS

Cell Culture

Tetracycline-inducible HEK293 human Flag-TRPM2–expressing cells were cultured at 37°C with 5% CO_2 in DMEM supplemented with 10% FBS. The medium was supplemented with blasticidin (5 μg/ml, Invitrogen) and zeocin (0.4 mg/ml, Invitrogen). For induction, cells were resuspended in medium containing 1 μg/ml tetracycline (Invitrogen) 5–20 h before experiments.

Solutions

For patch-clamp experiments, cells were kept in nominally divalent-free external solution (in mM, see also Table II): 140 NaCl, 11 glucose, 10 HEPES·NaOH (pH 7.2 adjusted with NaOH, 300 mOsm adjusted with sucrose). For some experiments, NaCl was equimolarly replaced by NMG-Cl (*N*-methyl-D-glucamine). Divalent cations (Ca^{2+}, Mg^{2+}, Zn^{2+}, Ba^{2+}, Sr^{2+}) were added as Cl^- salts into the standard external saline as described in the figures, or Ca^{2+} was buffered to near zero by adding 2 mM BAPTA. In some experiments, 1–2 μM thapsigargin or 2 μM calmidazolium (both Sigma-Aldrich) were added to the standard external saline, and cells were incubated for at least 15 min before experiments started. In others, 1 mM charbachol (Sigma-Aldrich) was added and cells superfused using the SmartSquirt delivery system (AutoMate Scientific), which included ValveLink TTL interface between the electronic valves and the EPC9 amplifier (HEKA). Since the SmartSquirt includes four separate chambers for application of different external solutions, this delivery system plus its digital interface to the EPC9 allowed for rapid and programmable solution changes via the PatchMaster software (HEKA). Standard pipette-filling solutions contained (in mM, see also Table I) 140 K-glutamate, 8 NaCl, 1 $MgCl_2$, 10 HEPES·KOH (pH 7.2 adjusted with KOH, 300 mOsm). $[Ca^{2+}]_i$ was buffered to 0, 30, 100, 300, or 1,000 nM with 10 mM BAPTA and 0, 1.2, 3.1, 5.7, or 8.2 mM $CaCl_2$, respectively, calculated with WebMaxC or left unbuffered (no buffer present). TRPM2 currents were activated by adding 1 mM ADPR (Sigma-Aldrich) to the pipette solution. For some experiments, pipette solutions were supplemented with 100–200 μM Sr^{2+} or 100 μM calmodulin (Sigma-Aldrich), and for perforated patch recordings, 300 μM amphotericin B (Sigma-Aldrich, freshly prepared from 30 mM stock in DMSO) was added.

Electrophysiology

Patch-clamp experiments were performed in the whole-cell configuration at 21–25°C. Patch pipettes were pulled from Kimax 1.5–1.8 × 100 mM glass capillaries (Kimble Products) on a DMZ-Universal Puller (Carl Zeiss MicroImaging, Inc.), and had resistances between 1.5 and 3 MΩ. Data were acquired with PatchMaster

TABLE II

Composition of Extracellular Solutions in mM

	nDVF	0 Ca	Nominal Ca	10 mM Mg	10 mM Sr	10 mM Ba	Zn	NMG	1 Ca	1 Ca 1 Ba	1 Ca 1 Mg
BAPTA	0	2	0	0	0	0	0	0	0	0	0
Divalent	0	0	n to 10 Ca	0	10 Sr	10 Ba	1–10 Zn	n to 10 Ca	1 Ca	1 Ca 1 Ba	1 Ca
$MgCl_2$	0	0	0	10	0	0	0	0	0	0	1
NaCl	140	140	140	140	140	140	140	0	140	140	140
NMG-Cl	0	0	0	0	0	0	0	120-140	0	0	0
HEPES	10	10	10	10	10	10	10	0	10	10	10

pH 7.2 (adjusted with NaOH or HCl); osmolarity, 300–310 mOsm (adjusted with sucrose), n = nominal.

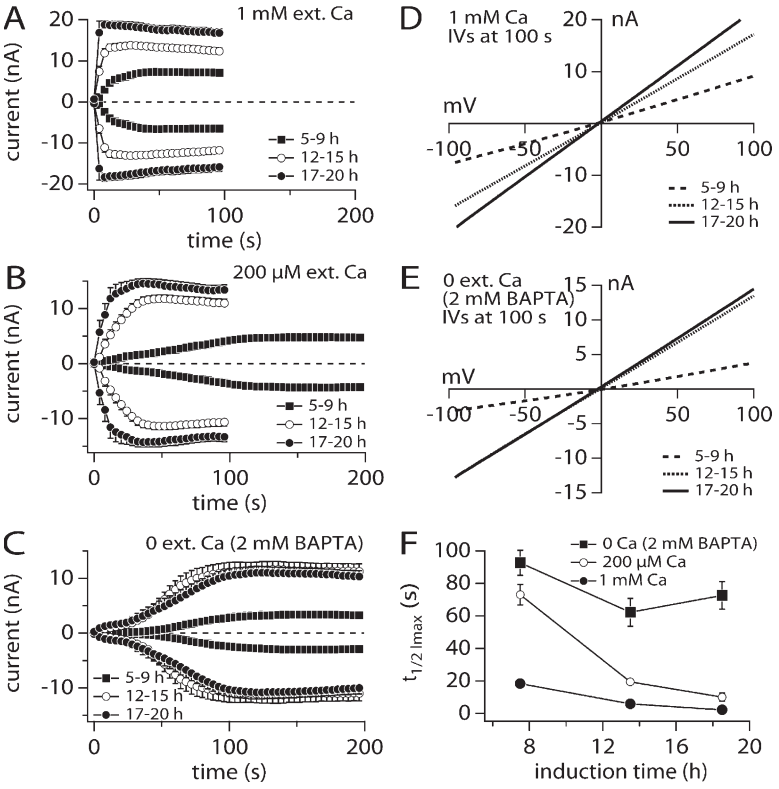

Figure 1. Induction time and external Ca influence activation kinetics of TRPM2. (A) Average current development of human TRPM2 inward and outward currents measured in HEK293 cells induced with tetracycline for different lengths of time (closed square 5–9 h, $n = 18$; open circles 12–15 h, $n = 24$; closed circles 17–20 h, $n = 6$). Currents were measured with a voltage ramp from −100 to +100 mV over 50 ms at 0.5-Hz intervals from a holding potential of 0 mV. Inward current amplitudes were extracted at −80 mV and outward currents at +80 mV, averaged, and plotted versus time with error bars representing SEM. Cells were perfused with the standard intracellular K^+-based solution in the absence of exogenous Ca^{2+} buffers and supplemented with 1 mM ADPR (see Table I). Standard extracellular solution contained 1 mM Ca^{2+}. (B) Averaged TRPM2 current development at different tetracycline induction times where extracellular Ca^{2+} concentration was lowered to 200 μM (closed square 5–9 h, $n = 24$; open circles 12–15 h, $n = 29$; closed circles 17–20 h, $n = 10$). Currents analyzed as in A. (C) Averaged TRPM2 current development at different tetracycline induction times in the absence of extracellular Ca^{2+} and addition of 2 mM BAPTA (closed square 5–9 h, $n = 14$; open circles 12–15 h, $n = 14$; closed circles 17–20 h, $n = 17$). Currents analyzed as in A. (D) Current–voltage (IV) relationship taken from representative cells kept in 1 mM extracellular Ca and at different tetracycline induction times. Data were extracted at 100 s into the experiment. (E) IV curves taken from representative cells kept in 0 mM extracellular Ca^{2+} and at different tetracycline induction times. Data were extracted at 100 s into the experiment. (F) Rates of activation ($t_{1/2}$ of I_{max}) plotted as a function of induction times from three different external Ca^{2+} levels: 0, closed squares; 0.2, open circles; and 1 mM, closed circles. N as noted in A–C. Error bars represent SEM.

software controlling an EPC-9 amplifier. Voltage ramps of 50 ms spanning the voltage range from −100 to +100 mV were delivered from a holding potential of 0 mV at a rate of 0.5 Hz, typically over a period of 100–400 s. Voltages were corrected for a liquid junction potential of 10 mV. Currents were filtered at 2.9 kHz and digitized at 100-μs intervals. Cells with access resistances >10 Mohm after whole-cell establishment (first measurement < 2 s) were not used for analysis and discarded. Capacitive currents and series resistance were determined and corrected before each voltage ramp. The low-resolution temporal development of currents for a given potential was extracted from the leak-corrected individual ramp current records by measuring the current amplitudes at voltages of −80 or +80 mV. For some experiments, the perforated patch clamp technique was used. Cells were kept in the cell-attached mode at a holding potential of −60 mV until the series resistance was <20 MΩ (typically within 10–15 min), then the ramp protocol (see above) was started.

Fura-2 Ca^{2+} Measurements

For Ca^{2+} measurements, cells were loaded with 1 μM Fura-2-AM (acetoxymethylester; Molecular Probes) for 30–60 min in media at 37°C, washed, and kept in external solution. In addition to preloading, Fura-2 (pentapotassium salt, Molecular Probes) was added to the standard internal solution at 50–100 μM. The cytosolic calcium concentration of individual patch-clamped cells was monitored at a rate of 5 Hz with a dual excitation fluorometric system using a Carl Zeiss MicroImaging, Inc. Axiovert 200 fluorescence microscope equipped with a 40× LD AchroPlan objective. The monochromatic light source (monochromator B, TILL-Photonics) was tuned to excite Fura-2 fluorescence at 360 and 390 nm for 20 ms each. Emission was detected at 450–550 nm with a photomultiplier, whose analogue signals were sampled and processed by X-Chart software (HEKA). Fluorescence ratios (F_{360}/F_{390}) were translated into free intracellular calcium concentration based on calibration parameters derived from patch-clamp experiments with calibrated Ca^{2+} concentrations.

Data Analysis

Data were analyzed with FitMaster (HEKA) and IgorPro (WaveMetrics). Where applicable, statistical errors of averaged data are given as means ± SEM with n determinations. Single ramps were plotted as current–voltage relationships (IVs).

RESULTS

Activation Kinetics of TRPM2 Depend on Tetracycline Induction Time and Extracellular Calcium

To obtain consistent TRPM2 expression levels suitable to derive quantitative assessments of current amplitudes in whole-cell recordings, we analyzed TRPM2 currents in HEK293 cells at various times between 5 and 20 h following tetracycline-induced expression. TRPM2-expressing cells were kept in a standard external Na^+ solution with varying Ca^{2+} concentrations and perfused with a standard internal K^+-glutamate–based solution that included 1 mM ADPR without any Ca^{2+} buffers (see Materials and methods). In Fig. 1 it is seen that extreme kinetic variations can occur under these conditions. These depend on induction times (Fig. 1 A) and on external Ca^{2+} levels (A–C). In Fig. 1 A, we divided the induction

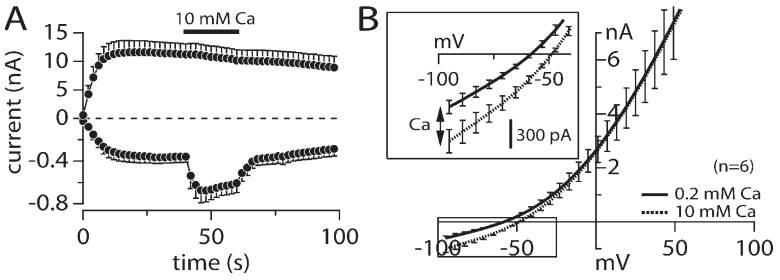

Figure 2. Calcium permeation of TRPM2 in external Na^+-free media. (A) Average current development of TRPM2 inward and outward currents measured in HEK293 cells induced with tetracycline for 7 h ($n = 6$ total). Voltage ramp and analysis as in Fig. 1. Cells were kept in an external solution where Na^+ was replaced with equimolar NMG plus 0.2 mM Ca^{2+} (see Table I). At 40 s into the experiment, the cell was superfused with a solution of similar composition but which now contained 10 mM Ca^{2+}. The black bar indicates application time. Patch pipette contained intracellular K^+-based solution in the absence of buffers and supplemented with 1 mM ADPR. Note that only inward currents are affected by the 10 mM Ca^{2+} application. (B) Comparison of averaged IV data obtained before application (0.2 mM Ca^{2+}) and after 10 s of application of 10 mM external Ca^{2+} ($n = 6$).

time into three groups including short (5–9 h), intermediate (12–15 h), and long induction durations (17–20 h). A comparison of the mean currents obtained from the three induction time groups exhibits differences in peak current and in activation kinetics.

As shown in Fig. 1 A, under normal physiological conditions (1 mM external Ca^{2+}), the peak current magnitude increased with longer induction times. With short induction times the mean peak current was 6.5 nA, which increased to 13 nA with intermediate induction times and further increased to 18 nA with the longest induction times. Presumably, the peak current variation is due to the different number of channels expressed as a function of induction time. At the same time, the kinetics of current activation accelerated with longer induction times. To assess activation kinetics, we measured the time to reach half-maximal current amplitude, which is referred to as $t_{1/2}$ (Fig. 1 F, closed circles). The value of $t_{1/2}$ was 18 s for short induction times, accelerated to 6 s with intermediate induction times, and became nearly instantaneous with longer induction times.

Fig. 1 B illustrates that TRPM2 activation by 1 mM ADPR was also dependent on the external Ca^{2+} concentration. Decreasing external Ca^{2+} levels from 1 to 0.2 mM or removing Ca^{2+} completely (nominally Ca^{2+}-free conditions) slowed the rate of activation. With short, intermediate, and long induction time groups, the activation kinetics with 0.2 mM external Ca^{2+} were 73, 20, and 10 s, respectively (Fig. 1, B and F, open circles). Removal of external Ca^{2+} (Fig. 1 C) further slowed the activation of TRPM2 currents across induction times. With short, intermediate, and long induction times $t_{1/2}$ values were 93, 62, and 73 s, respectively (Fig. 1 F, closed squares).

Since TRPM2 is a Ca^{2+}-permeable cation channel, endogenously expressed Ca^{2+}-dependent channels in HEK293 cells, notably TRPM4 (Launay et al., 2002), could contribute to the currents observed here. However, their overall contribution is likely to be minimal, since TRPM4 peak amplitudes do not exceed 200 pA at −80 mV and exhibit S-shaped current–voltage (IV) relationships with slight outward rectification. TRPM2 inward and outward currents typically exceeded several nA and are symmetrical, as seen in Fig. 1 (A–C). In Fig. 1 (D and E), IV curves were plotted from various experimental conditions and illustrates this linearity between inward and outward currents. The IV data are plotted at 100 s of current development with different induction times and different external Ca^{2+} concentrations of 1 mM (Fig. 1 D) or 0 external Ca^{2+} (Fig. 1 E). The IVs from both external Ca^{2+} levels are identical except for current magnitude, which varies due to different channel number expressed at varying induction times. Since IVs are identical we can assume that the data arise primarily from TRPM2 with negligible contributions of endogenous channels.

The activation kinetics observed at different levels of external Ca^{2+} as a function of varying induction times are summarized in Fig. 1 F. With 1 mM external Ca^{2+}, the activation times at different induction times are relatively fast (closed circle). However, with a lower concentration of 0.2 mM Ca^{2+} (open circles), the activation is strongly dependent on induction time. In contrast, with 0 external Ca^{2+} (closed squares), activation is slower and does not change significantly with different induction times. We conclude that extracellular Ca^{2+} levels significantly influence TRPM2 activation kinetics. Since TRPM2 is a Ca^{2+}-permeable cation channel (Perraud et al., 2001; Sano et al., 2001; Hara et al., 2002), the effects seen on the channel kinetics could be due to external or internal interaction sites for Ca^{2+}. To optimize consistency in our dataset, further experiments were conducted with cells induced for 12–15 h unless indicated otherwise in the text.

Ca^{2+} Permeation Is Preserved when Substituting Na^+ with NMG

Due to TRPM2's permeability to Ca^{2+}, the intracellular accumulation of this ion may be an important divalent cation for TRPM2 channel modulation. This Ca^{2+} influx can be assessed directly in the absence of extracellular Na^+. In these experiments (Fig. 2 A), TRPM2 currents were activated by 1 mM ADPR while keeping external Ca^{2+} concentration at 0.2 mM. After full activation of TRPM2 current, external Ca^{2+} concentration was increased to 10 mM Ca^{2+}. This rapid change from low to a higher Ca^{2+} level resulted in an instantaneous increase of the inward current at −80 mV with no

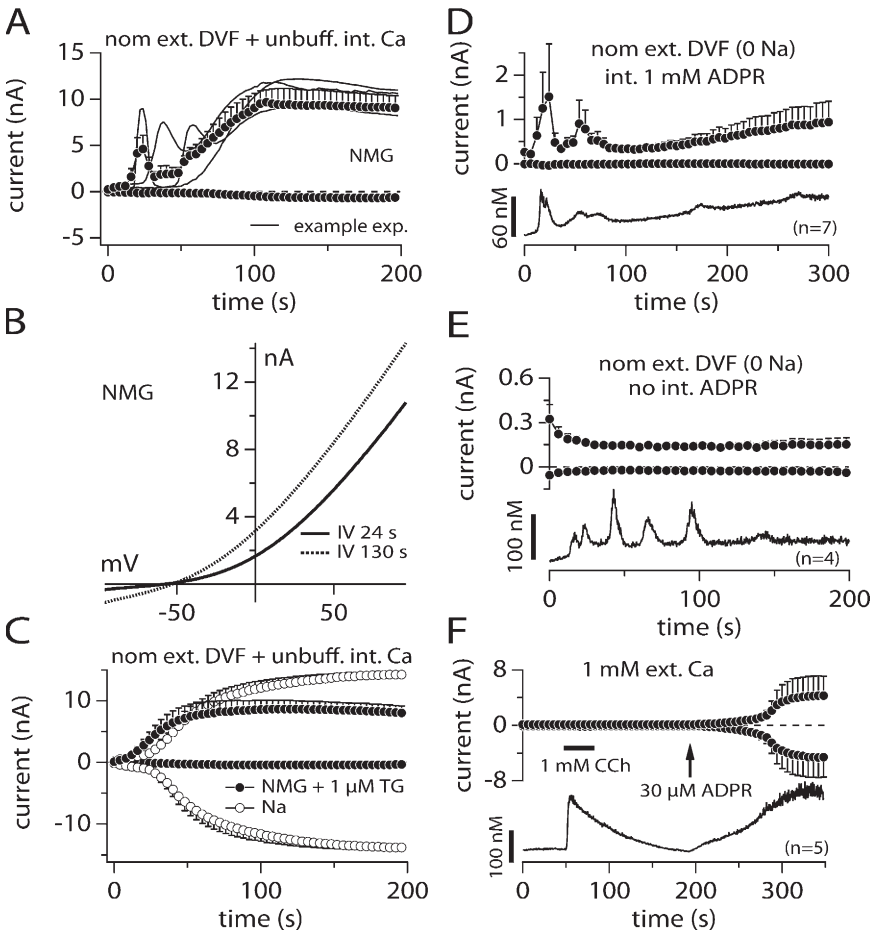

Figure 3. Replacing external Na^+ with NMG introduces current oscillations. (A) Average current development of human TRPM2 inward and outward currents measured in NMG-based solution with nominally divalent-free (nDVF; no exogenous buffers; $n = 7$) and unbuffered intracellular K^+-based solution supplemented with 1 mM ADPR. Currents acquired and analyzed as in Fig. 1. Error bars represent SEM. Gray lines represent three of the seven recorded cells. Cells were tetracycline induced between 12 and 15 h. Note that inward currents are absent due to the absence of extracellular TRPM2-permeating ions (Na^+ and Ca^{2+}). Outward currents are carried by K^+ ions. (B) IV curves taken from a representative cell kept in nDVF-NMG solution as indicated in A. The IV data were obtained from the oscillating current at its peak magnitude (24 s) and from the steady-state level (130 s). (C) Oscillations are removed in the presence of extracellular Na^+ (open circles, $n = 15$) or addition of 1 μM thapsigargin to the NMG-based solution to induce Ca^{2+} release (closed circles, $n = 8$). The panel shows average current development of TRPM2 induced by 1 mM ADPR in these two conditions. Error bars are SEM. (D) The graph shows average TRPM2 currents induced by 1 mM ADPR (top panel closed circles, $n = 7$) and corresponding intracellular Ca^{2+} signals (bottom panel, continuous line, $n = 7$) measured simultaneously in the whole-cell configuration. Data acquisition and analysis for currents as described in Fig. 1. Cells were kept in nominal divalent-free (DVF) and Na^+-free (NMG) external saline (see Table I). 50 μM Fura-2 was added to the pipette filling solution. Currents and Ca^{2+} signals are developing in parallel to each other. (E) Depicted are average whole-cell current measurements (top, closed circles, $n = 4$) and corresponding intracellular Ca^{2+} signals (bottom, continuous line, $n = 4$) in tetracycline-induced TRPM2-overexpressing HEK293 cells but in the absence of intracellular ADPR. Acquisition and analysis as described in D. Note the absence of TRPM2 currents despite prominent Ca^{2+} oscillations. (F) Concurrent current and intracellular Ca^{2+} measurements using the perforated-patch technique followed by rupture of patch and perfusion of cell with 30 μM ADPR and Fura-2 as indicated by the arrow ($n = 5$). Cells were preloaded with Fura2-AM (see Materials and methods). Cells were first kept in the cell-attached mode and at a holding potential of −60 mV. The pipette contained the ionophore amphotericin B (300 μM). Establishment of perforated-patch configuration was determined when the series resistance reached 20 MΩ and less. After establishment of the perforated patch voltage ramps were acquired. External application of 1 mM charbachol (CCh) as indicated by the black bar. When intracellular Ca^{2+} levels had fallen back to basal levels after CCh stimulation, the perforated patch was ruptured to establish the whole cell mode (see arrow) and TRPM2 currents could be recorded.

change in the outward current at +80 mV. The IV data comparison between 0.2 Ca^{2+} and 10 mM Ca^{2+} (Fig. 2 B) shows a difference in the mean inward current of 330 pA. These results clearly show that TRPM2 can sustain a relatively small, but measurable inward Ca^{2+} current in the absence of any other permeating ion species.

Absence of Extracellular Na^+ Induces Ca^{2+} Oscillations Independent of ADPR

As shown in Fig. 2, ADPR evoked TRPM2 currents under Na^+-free and low Ca^{2+} conditions. Interestingly, when removing external Na^+ ions (replaced by NMG) under nominally divalent-free (nDVF) conditions, TRPM2 currents started to oscillate during the first 100 s in almost all of the cells investigated (Fig. 3 A). This oscillating response occurred only when perfusing cells with ADPR and in the absence of external Na^+ with nominal or zero external Ca. Currents never activated in the absence of ADPR in 0 Na^+ conditions (Fig. 3 E, top). With ADPR, usually one or two initial transient responses occurred and these were followed by a larger sustained current, with no apparent oscillations. Fig. 3 A superimposes three individual records together with their statistical mean and Fig. 3 B shows two example IVs obtained during the peak of a current transient (24 s) and during the sustained phase (130 s). Aside from the current amplitude, these IVs were identical in shape and reversal potential (E_{rev} = −57 and −53 mV, respectively).

Given the sensitivity of TRPM2 to intracellular Ca^{2+} and the fact that both current development and oscillations

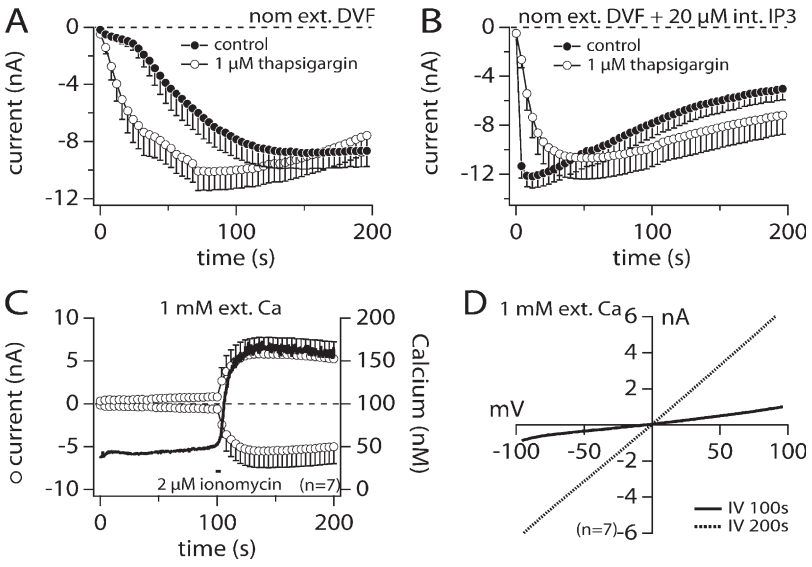

Figure 4. Thapsigargin, IP_3, and ionomycin enhance ADPR-induced TRPM2 activation. (A) Average current development of human TRPM2 inward currents measured in HEK293 cells in the absence (closed circles, $n = 17$) or presence of 1 μM thapsigargin in the bath medium (open circles, $n = 13$). Currents acquired and analyzed as in Fig. 1. Error bars represent SEM. Cells were perfused with the standard intracellular K^+-based solution in the absence of exogenous Ca^{2+} buffers and supplemented with 1 mM ADPR. Extracellular solution was nominally divalent free (nDVF). (B) Averaged TRPM2 current development by 1 mM ADPR in the presence of 20 μM intracellular IP_3 (closed circles, $n = 15$). The addition of 1 μM thapsigargin to the bath medium (open circles, $n = 11$) did not significantly change TRPM2 activation kinetics compared with IP_3 supplement alone. (C) TRPM2 currents (open circles, left axis) and corresponding intracellular Ca^{2+} signals (solid trace, right axis) induced by 1 mM intracellular ADPR are shown from cells kept in external saline containing 1 mM Ca^{2+} ($n = 7$). 100 μM Fura-2 was added to the pipette filling solution. After reaching whole cell configuration, TRPM2 currents developed very slowly possibly due to the mild buffering capacity of Fura-2. When applying 2 μM ionomycin in 0 Ca^{2+} medium (indicated by the black bar) intracellular Ca^{2+} increased with a parallel fast recruitment of TRPM2 currents. (D) The graph shows IVs extracted from a representative cell at different times into the experiment.

were only present when cells were perfused with ADPR, we wondered whether the oscillations resulted from release of Ca^{2+} from internal stores induced by either the absence of extracellular Na^+ or by ADPR itself. To test for possible Ca^{2+} release effects, we initially added 1 μM of the sarco/endoplasmatic calcium ATPase (SERCA) pump inhibitor thapsigargin to the external NMG solution. With thapsigargin treatment, external NMG no longer induced these early oscillating currents (Fig. 3 C). Fig. 3 C also demonstrates that regular Na^+-based media prevented the oscillating responses even in Ca^{2+}-free conditions. These data suggest that under Na^+-free experimental conditions, perfusion of cells with ADPR results in Ca^{2+} release, which in turn causes transient TRPM2 activation.

To visualize and determine the temporal relationship between Ca^{2+} release and the development of current in NMG media we used combined Fura-2 Ca^{2+} imaging and patch-clamp experiments. In Fig. 3 D, with external NMG solution and with 1 mM internal ADPR we observed clear correspondence of Ca^{2+} release (bottom) and current development (top), as both events proceeded in parallel. During the first 100 s, Ca^{2+} release and current development was transient and was followed by an accumulation of $[Ca^{2+}]_i$ and the development of a steady-state current.

In Fig. 3 E, we performed experiments under the same experimental conditions but eliminated internal ADPR. Under these conditions, we also observed Ca^{2+} release from internal stores during the first 100 s (bottom), but this was not accompanied by a parallel development of current, presumably due to the absence of ADPR. Although these results do not exclude that ADPR may contribute to Ca^{2+} release from intracellular stores, they indicate that Ca^{2+} release does not require ADPR and may be induced by the combined experimental conditions, i.e., absence of permeating Na^+ and/or presence of external NMG and/or perfusion of cells with standard internal saline. However, the combined presence of ADPR and elevated $[Ca^{2+}]_i$ ultimately is responsible and required for transient and sustained activation of TRPM2.

It has recently been proposed that mobilization of internal Ca^{2+} is sufficient to activate TRPM2 current with resting levels of internal ADPR (Heiner et al., 2006). To address the question of whether TRPM2 is activated by internal Ca^{2+} or by ADPR in HEK293 cells, we performed combined perforated-patch and Fura-2 experiments. Intact cells were preloaded with Fura-2- AM to monitor $[Ca^{2+}]_i$, and patch pipettes contained 300 μM amphotericin B for perforated patch recordings for the first 200 s of the experiment. Upon establishment of voltage-clamp conditions through the perforated patch, considered adequate after the series resistance was <20 MΩ, currents and Ca^{2+} levels were acquired simultaneously (top and bottom panels, respectively). 50 s into the experiment, cells were stimulated with 1 mM carbachol (CCh) to induce internal Ca^{2+} release. This resulted in a clear Ca^{2+} release transient but no parallel development of current. Patch pipettes also contained Fura-2 and 30 μM ADPR, enabling us to rupture the perforated patch and establish classical whole-cell conditions, while continuing to monitor $[Ca^{2+}]_i$ and at the same time assessing the effects of ADPR introduction into the cell. Upon rupturing the perforated patch and thus introducing 30 μM ADPR into the cell (see arrow),

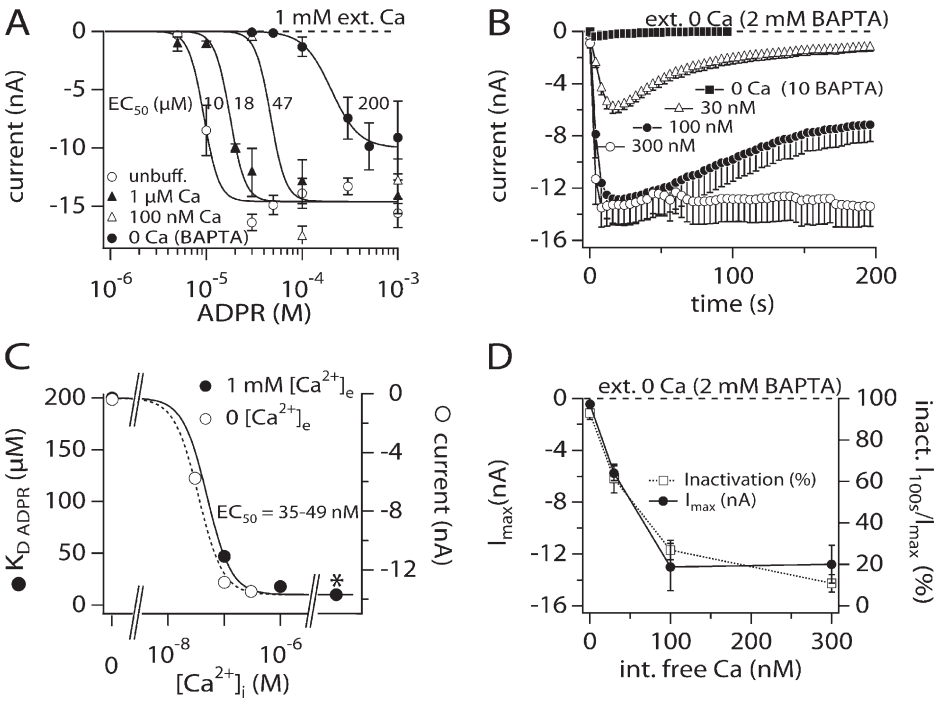

Figure 5. Ca^{2+} facilitates ADPR-induced TRPM2 recruitment and modulates current kinetics. (A) Dose–response curves of ADPR-induced TRPM2 currents measured in HEK293 cells bathed in regular external saline supplemented with 1 mM Ca^{2+} in response to increasing intracellular Ca^{2+} concentrations or unbuffered K^+-based internal solution: 0 Ca, closed circles, n = 3–8; 100 nM Ca^{2+}, open triangles, n = 5–6; 1 μM, closed triangles, n = 4–11; unbuffered, open circles, n = 3–13. Data were fitted with dose–response curves (see Materials and methods) and the EC_{50}s established as indicated in the panel. Hill coefficients were 5.5 for unbuffered, 1 μM, and 100 nM Ca^{2+} and 3 for 0 Ca^{2+} (BAPTA). Data were acquired as described in Fig. 1. To establish the dose–response curves, the maximum inward currents in response to ADPR and measured at −80 mV were extracted, averaged, and plotted versus the respective ADPR concentration. Tetracycline induction time was between 12 and 15 h. (B) The graph shows the average TRPM2 development in response to 1 mM ADPR and different levels of internal Ca^{2+} while maintaining external Ca^{2+} at 0 mM in the presence of BAPTA (0 Ca^{2+}, closed squares, n = 7; 30 nM Ca^{2+}, open squares, n = 14; 100 nM Ca^{2+}, closed circles, n = 6; 300 nM, open circles, n = 6). Fixed Ca^{2+} levels were established by using 10 mM BAPTA with an appropriate concentration of $CaCl_2$ as calculated by WebmaxC (see Materials and methods). Data acquisition and analysis as in Fig. 1. Error bars represent SEM. (C) The graph displays the sensitivity of TRPM2 to increasing intracellular Ca^{2+} concentrations in the presence (1 mM, closed circles) or absence (2 mM BAPTA, open circles) of extracellular Ca^{2+}. Intracellular ADPR was 1 mM. For 1 mM extracellular Ca^{2+} the EC_{50} values for ADPR were plotted against their respective intracellular Ca^{2+} concentration. Data were taken from A. A dose–response fit to the curve showed that the half-maximal activation capacity of Ca^{2+} is at 49 nM with a Hill coefficient of 2. The data acquired in 0 external Ca^{2+} are plotted as the maximum current amplitude in response to increasing intracellular fixed Ca^{2+} as taken from B. A dose–response fit to these data gave an EC_{50} value of 34 nM with a Hill coefficient of 2. The asterisk indicates unbuffered Ca^{2+} conditions (~5 μM). (D) The graph summarizes the results of B plotting both I_{max} and % inactivation as a function of intracellular Ca^{2+} levels. Note that both the level of inactivation and the level of maximum current develop in a parallel manner.

the TRPM2 current develops in parallel with intracellular Ca^{2+} levels. These experiments clearly demonstrate that intracellular Ca^{2+} release with basal levels of ADPR does not activate the TRPM2 currents in TRPM2-overexpressing HEK293 cells. Activation of TRPM2 current occurs only when ADPR levels increase above the basal concentration plus the accumulation of internal Ca^{2+}.

Intracellular Ca^{2+} Facilitates ADPR-mediated Activation of TRPM2

The above data indicate that intracellular $[Ca^{2+}]_i$ facilitates ADPR-induced TRPM2 activation. Classical intracellular Ca^{2+}-increasing agents are the SERCA pump inhibitor thapsigargin, the calcium release agent inositol 1,4,5 trisphosphate (IP_3), and the calcium ionophore ionomycin. We wondered whether exposure of TRPM2-expressing HEK293 cells to 1 μM thapsigargin in nominally divalent-free extracellular solution conditions would accelerate ADPR-induced TRPM2 recruitment compared with control. Indeed, TRPM2 activated faster in the presence of the SERCA pump inhibitor (Fig. 4 A, open circles) than under control conditions (Fig. 4 A, closed circles), further indicating a facilitatory role of $[Ca^{2+}]_i$. Furthermore, perfusing cells with 20 μM IP_3 in addition to 1 mM ADPR caused an almost instantaneous and maximal activation of TRPM2 (Fig. 4 B, closed circles) that was not significantly altered by the additional presence of 1 μM thapsigargin in the bath (Fig. 4 B, open circles). Finally, concurrent measurements of TRPM2 whole-cell currents and $[Ca^{2+}]_i$ using Fura-2 revealed that an increase of $[Ca^{2+}]_i$ induced by application of 2 μM ionomycin from the outside of the cell (Fig. 4 C, solid trace and right axis) strongly enhanced the TRPM2 current amplitude (Fig. 4 C, open circles and left axis), clearly correlating intracellular Ca^{2+} increases to TRPM2 facilitation in the presence of ADPR. The corresponding IV curves are shown in Fig. 4 D.

To further characterize the facilitatory effect of $[Ca^{2+}]_i$ on ADPR-induced TRPM2 activation, we constructed several complete ADPR dose–response curves at four different intracellular Ca^{2+} concentrations in the presence of physiological extracellular Ca^{2+} (1 mM) and intracellular K^+. Fig. 5 A demonstrates that the ADPR sensitivity of TRPM2 increases with increased internal calcium levels.

For example, under unbuffered $[Ca^{2+}]_i$, the half-maximal effective concentration (EC_{50}) of ADPR is ~10 μM. This is shifted to 47 μM at 100 nM fixed $[Ca^{2+}]_i$, and further shifted to 200 μM at 0 $[Ca^{2+}]_i$. Plotting these EC_{50} values against their respective Ca^{2+} concentrations and fitting a dose–response curve to the data points yields an EC_{50} value for $[Ca^{2+}]_i$ of 50 nM (Hill = 2; Fig. 5 C). This means that 50% efficiency of Ca^{2+}-induced facilitation of gating by ADPR is already reached at low basal Ca^{2+} levels in the presence of K^+ ions.

We next determined whether the dose–response behavior of ADPR-induced TRPM2 to Ca^{2+} is partially modulated by extracellular Ca^{2+}. We therefore constructed a Ca^{2+} dose–response curve at a fixed level of ADPR (1 mM) while removing external Ca^{2+} and additionally adding 2 mM BAPTA (Fig. 5 B). As can be seen, while the complete absence of extra- and intracellular Ca^{2+} prevents channel activation, as little as 30 nM $[Ca^{2+}]_i$ already causes 50% of current activation in the complete absence of extracellular Ca^{2+}. Furthermore, plotting the peak current amplitudes against their respective fixed internal Ca^{2+} concentration and fitting a dose–response curve to the data yields an EC_{50} value for $[Ca^{2+}]_i$ of 35 nM (Hill coefficient of 2; Fig. 5 C). Since this value is very similar to that obtained in the presence of 1 mM external Ca^{2+}, this result indicates that extracellular Ca^{2+} does not significantly contribute to Ca^{2+}-dependent regulation of TRPM2 and that an intracellular mechanism is primarily responsible. In addition to affecting current magnitudes, $[Ca^{2+}]_i$ at or below 100 nM induces a prominent current inactivation (Fig. 4 B) that diminishes in parallel with increased TRPM2 current amplitude (Fig. 5 D).

Extracellular Ca^{2+} Plays an Important Role in Channel Function

Why can ADPR gate TRPM2 in the absence of internal Ca^{2+} but not in the absence of both internal and external Ca^{2+} (Fig. 5 B; Fig. 6 A)? From the data in Fig. 5 (B and D) it appears that TRPM2 completely inactivates in the absence of extra- and intracellular Ca^{2+}, thus preventing ion permeation. Alternatively, the channel could have an additional Ca^{2+} interaction site facing the extracellular milieu that needs to be occupied for channel function. To test these two hypotheses, we measured the current development at different external Ca^{2+} concentrations (nominal DVF [estimated ~5 μM], 200 μM, and 1 mM) and at increasing intracellular Ca^{2+} levels (0, 30 nM, and unbuffered), using a fixed ADPR concentration of 1 mM (Fig. 6, A–C). With the combination of zero internal Ca^{2+} and nDVF, activation of TRPM2 is very small (Fig. 6 A, inset). Increasing the external Ca^{2+} concentration to 200 μM in combination with zero internal Ca^{2+} doubles the magnitude of the current to 500 pA and shows a clear component of inactivation that shuts the current down within 100 s (Fig. 6 A, inset). Additional increases in the external Ca^{2+} to 1 mM in combination with zero internal Ca^{2+} produces a mean current that reaches a mean amplitude of 8 nA, i.e., only half of the mean maximum current of 14–18 nA achievable with 1 mM external Ca^{2+} and unbuffered internal Ca^{2+} (Fig. 1 A and Fig. 6 C, closed circles). These data confirm that at Ca^{2+} concentrations <100 nM, TRPM2 currents not only fail to reach maximal amplitudes, but also undergo prominent inactivation. However, as can be seen in Fig. 6 (A and B), the kinetics and extent of current inactivation is not altered when increasing extracellular Ca^{2+} from nDVF to 1 mM. Hence, extracellular Ca^{2+} seems to have little influence over both TRPM2 inactivation kinetics and Ca^{2+}-facilitated ADPR gating.

However, extracellular Ca^{2+} seems mandatory for TRPM2 gating when intracellular Ca^{2+} is depleted (Fig. 5 B and Fig. 6 A). This indicates that the ion channel has an additional Ca^{2+} interaction site facing the extracellular milieu that can rescue channel function. To further test this hypothesis, we bathed cells in the standard 1 mM Ca^{2+}-containing external solution and perfused cells with 1 mM ADPR and 0 Ca^{2+} (10 mM BAPTA). Once TRPM2 currents had fully developed, we superfused cells with a solution that contained no divalent ions plus 100 μM BAPTA as indicated in Fig. 6 D. The removal of Ca^{2+} caused a fast and prominent closure of TRPM2 currents with a time constant of 4 s that did not reverse upon reintroduction of extracellular Ca^{2+} (not depicted). Both inward (Fig. 6 D) and outward currents (not depicted) show the same rate of inactivation. This rate of inactivation is approximately four times faster than in control cells without application, where the rate of inactivation proceeded with a time constant of 19 s. The rate of inactivation was assessed by fitting a single exponential function between 36 and 100 s for control cells and between 32 and 48 s for DVF conditions (Fig. 6 D).

To determine whether this effect was solely due to Ca^{2+} or whether other divalent ions could replace this ion, we performed the same experiments but substituted Ca^{2+} with 1 mM Mg^{2+} or 1 mM Ba^{2+}. The inactivation time constant in the absence of Ca^{2+} but presence of Mg^{2+} was approximately five times faster than control conditions (no application) with $\tau = 2$ s and $\tau = 11$ s, respectively (Fig. 6 E), for both inward and outward currents. Furthermore, removing extracellular Ca^{2+} in the continued presence of 1 mM Ba^{2+} also inactivated TRPM2 currents with a time constant of 2 s, approximately seven times faster than control conditions (Fig. 6 F) for both inward and outward currents. The presence of extracellular Ca^{2+} was mandatory to cause TRPM2 activation after whole-cell establishment while perfusing the cell with 1 mM ADPR in 0 intracellular Ca^{2+} solution (10 mM BAPTA), since TRPM2 currents did not develop in cells that were kept in a Na^+-based saline where Ca^{2+} was replaced with either 1 mM Mg^{2+} or 1 mM Ba^{2+} (Fig. 6 G; see Table II for solutions).

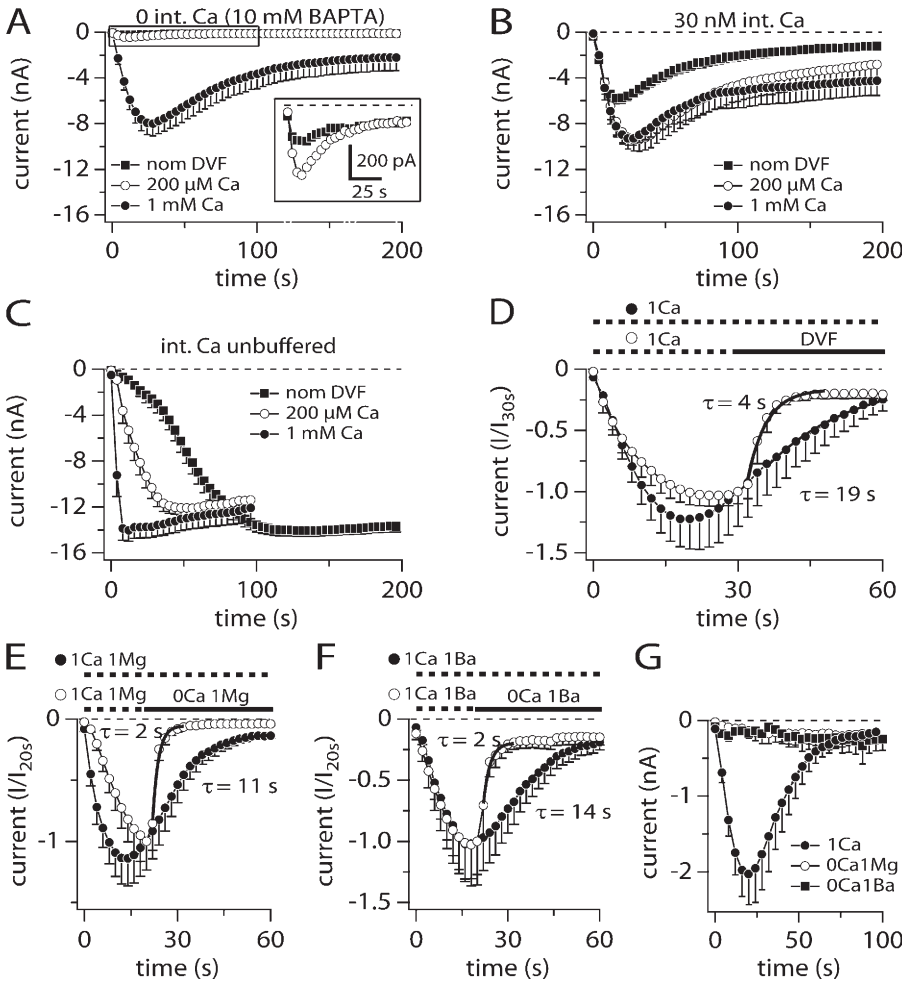

Figure 6. Effects of extracellular Ca^{2+}. (A) Average current development of TRPM2 inward currents at −80 mV in response to perfusion with 1 mM ADPR in the absence of intracellular Ca^{2+} and in increasing extracellular Ca^{2+} concentrations with nDVF (closed squares, $n = 31$), 200 µM (open circles, $n = 15$), or 1 mM Ca^{2+} (closed circles, $n = 24$). Error bars represent SEM. (B) Average TRPM2 development of inward currents in response to 1 mM ADPR at 30 nM fixed intracellular Ca^{2+} and in increasing extracellular Ca^{2+} concentrations with nDVF (closed squares, $n = 9$), 200 µM (open circles, $n = 4$), or 1 mM Ca^{2+} (closed circles, $n = 14$). Error bars represent SEM. (C) Average TRPM2 development of inward currents in response to 1 mM ADPR in unbuffered intracellular Ca^{2+} conditions and with increasing extracellular Ca^{2+} concentrations with nDVF (closed squares, $n = 14$), 200 µM (open circles, $n = 10$), or 1 mM Ca^{2+} (closed circles, $n = 7$). Error bars represent SEM. (D) Average time course of TRPM2 activation induced by 1 mM ADPR and 0 Ca^{2+} in the intracellular solution (10 mM BAPTA). Control cells were kept in a NaCl-based solution supplemented with 1 mM Ca^{2+} (closed circles, dashed lines, $n = 7$). In experimental cells Ca^{2+} was removed (DVF) at the time indicated by the black bar (open circles, $n = 5$). The rate of inactivation was assessed by fitting a single exponential function ($I \cdot \exp^{(-t/\tau)}$ + Amplitude) between 36 and 100 s for control cells and between 32 and 48 s for DVF conditions. (E) Average time course of TRPM2 activation induced as in D. Control cells were kept in a NaCl-based solution supplemented with 1 mM Ca^{2+} and 1 mM Mg^{2+} (closed circles, dashed lines, $n = 11$). In experimental cells only Ca^{2+} was removed at the time indicated by the black bar (open circles, $n = 11$). The rate of inactivation was assessed at the times indicated in D. (F) Average activation of TRPM2 induced as in D. Control cells were kept in a NaCl-based solution supplemented with 1 mM Ca^{2+} and 1 mM Ba^{2+} (closed circles, dashed lines, $n = 6$). In experimental cells again only Ca^{2+} was removed at the time indicated by the black bar (open circles, $n = 5$). The rate of inactivation was assessed between 22 and 32 s for experimental cells. (G) Average activation of TRPM2 induced as in D. Cells were kept in a NaCl-based solution supplemented with either 1 mM Ca^{2+} (closed circles, $n = 7$), 1 mM Mg^{2+} (open circles, $n = 8$), or 1 mM Ba^{2+} (closed squares, $n = 3$). Note the absence of current recruitment in the absence of Ca^{2+}.

Strontium Mimics Ca^{2+}-induced Facilitation of TRPM2

TRPM2 does not activate in the absence of intra- and extracellular Ca^{2+}, even in the presence of substituting divalent ions such as Mg^{2+} or Ba^{2+}. We wondered whether these divalent cations would also affect TRPM2 activation if intracellular Ca^{2+} were left unbuffered (0 BAPTA). To this end, we replaced external Ca^{2+} with different divalent ions including Sr^{2+}, Mg^{2+}, Zn^{2+}, and Ba^{2+} at a concentration of 10 mM in the bath solution (Fig. 7 A) and perfused the cells with 1 mM ADPR in the absence of internal calcium buffers. Extracellular Zn^{2+} totally blocked the channels. In contrast, external Mg^{2+} had no effect and showed similar kinetic behavior as the nDVF solution. External Ba^{2+} showed a similar activation as nDVF; however, Ba^{2+} introduced a delayed inactivation. Of the various divalents that were examined, only external Sr^{2+} appeared to substitute for Ca^{2+} in that it exhibited a similar effect on TRPM2 activation kinetics.

To determine whether Sr^{2+} regulation occurred internally similar to Ca^{2+}, we tested different concentrations of internal Sr^{2+} in combination with external media free of divalent cations (Fig. 7 B). In the presence of 1 mM ADPR, the efficacy for internal Sr^{2+} to facilitate TRPM2 gating was quite different from that seen with internal Ca^{2+}. The concentration to activate half of the maximal TRPM2 current required 1 µM Sr^{2+} (Fig. 7 B, closed circles), whereas only 30 nM is sufficient in the case of Ca^{2+} (Fig. 5 B, open triangle).

In the next series of experiments we attempted to answer the question of whether internal Sr^{2+} has a direct or an indirect effect on TRPM2 activation. One possible mechanism could be that Sr^{2+} induces Ca^{2+} release

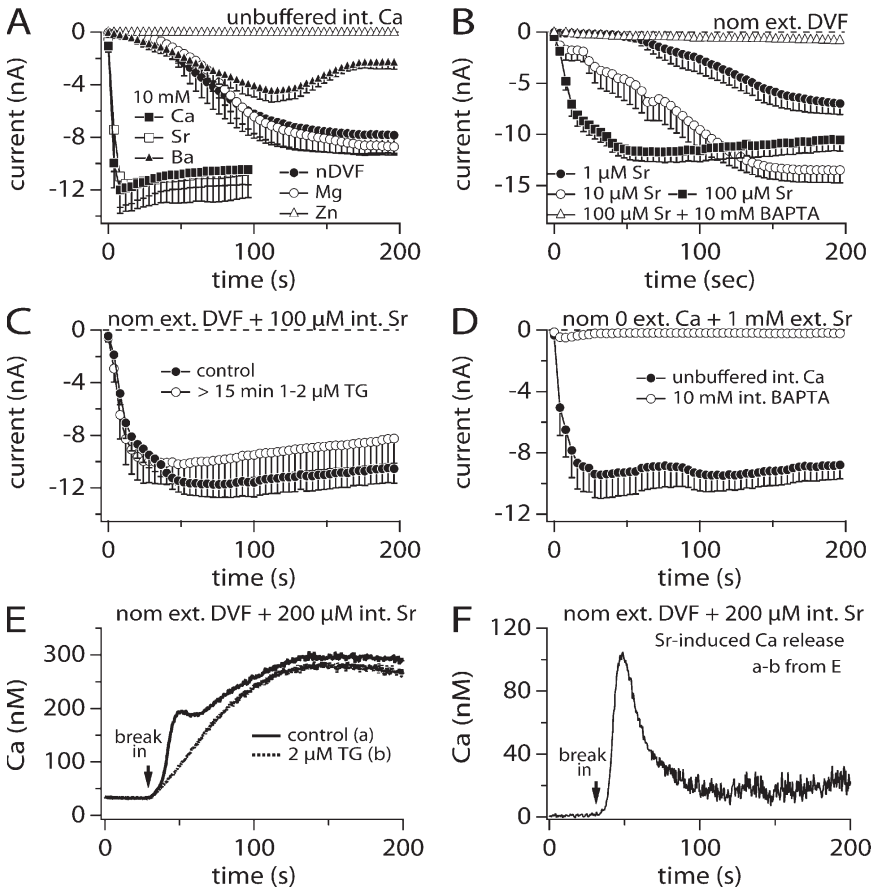

Figure 7. Substitution of Ca^{2+} with other divalent ions. (A) Average inward TRPM2 currents acquired in the presence of various individual extracellular divalent cations (10 mM) and plotted versus time. Currents were evoked by supplementing the unbuffered intracellular K^+-based saline with 1 mM ADPR. Shown are data for nominally divalent-free conditions (closed circles, $n = 7$), 10 mM Mg^{2+} (open circles, $n = 10$), 10 mM Zn^{2+} (open squares, $n = 9$), 10 mM Ba^{2+} (closed triangles, $n = 21$), 10 mM Ca^{2+} (closed squares, $n = 7$), and 10 mM Sr^{2+} (open squares, $n = 5$). (B) Activation of TRPM2 inward currents in dependence of increasing intracellular Sr^{2+} concentrations at fixed 1 mM ADPR and in the absence of extracellular Ca^{2+} (nDVF, $n = 4$–14). Intracellular Ca^{2+} was left unbuffered except in part of the dataset containing 100 μM Sr^{2+} (open triangles). Error bars indicate SEM. (C) Recruitment of TRPM2 inward currents by 1 mM ADPR and 100 μM Sr^{2+} in nDVF conditions (closed circles, $n = 14$, same data as in B). The presence of 1–2 μM thapsigargin in the extracellular medium did not alter activation kinetics further (open circles, $n = 8$). (D) TRPM2 activation in extracellular 1 mM Sr^{2+} while keeping intracellular Ca^{2+} unbuffered (closed circles, $n = 11$) or at 0 by addition of BAPTA (open circles, $n = 8$). Pipette solution contained 1 mM ADPR. (E) Ca^{2+} signal evoked in TRPM2-expressing HEK293 cells bathed in nDVF media and perfused with 200 μM Sr^{2+} in the absence (solid line, $n = 5$) or presence (dashed line, $n = 8$) of 2 μM external thapsigargin. K^+-based intracellular solution was further supplemented with 100 μM Fura-2 but did not contain any ADPR to avoid TRPM2 recruitment. Sr^{2+} caused an increase in the Ca^{2+} background signal that was identical in the presence or absence of thapsigargin. Cells were preloaded with FuraAM ester. (F) To isolate the Sr^{2+}-induced Ca^{2+} release from the Sr^{2+}-induced fluorescent background changes, the traces gathered in E were subtracted and plotted versus time.

from internal stores, since 100 μM Sr^{2+} plus ADPR in the pipette failed to activate a current when intracellular Ca^{2+} was buffered to near zero by 10 mM BAPTA (Fig. 7 B, open triangles). To test for this we compared current activation measured in the presence of internal 100 μM Sr^{2+} (Fig. 7 B, closed squares, and Fig. 7 C, closed circles) with records obtained in the absence of Sr^{2+} but treated with 1–2 μM thapsigargin, a SERCA pump inhibitor that leads to accumulation of cytosolic Ca^{2+} (Fig. 7 C, open circles). Both conditions showed no difference in the activation kinetics (Fig. 7 C), suggesting that Sr^{2+} may lead to cytosolic Ca^{2+} accumulation in a manner similar to thapsigargin, possibly by causing Sr^{2+}-induced Ca^{2+} release from internal stores.

If Sr^{2+} indeed leads to Ca^{2+} release from intracellular stores, then ADPR-induced (1 mM) TRPM2 activation in the presence of extracellular Sr^{2+} should be preventable by buffering Ca^{2+} to zero using BAPTA in the pipette (similar as shown in Fig. 7 B, open triangles). Fig. 7 D shows that unlike Ca^{2+}, external Sr^{2+} (1 mM) failed to support TRPM2 activation when buffering $[Ca^{2+}]_i$ to zero (Fig. 7 D, open circles), whereas in unbuffered conditions, where Ca^{2+} release may occur and elevate $[Ca^{2+}]_i$, TRPM2 is strongly activated in the presence of extracellular Sr^{2+}.

To substantiate and quantify Sr^{2+}-induced Ca^{2+} release from internal stores we used combined patch-clamp and balanced Fura-2 Ca^{2+} measurements. Here, the cells were preloaded with Fura-2-AM ester (see Materials and methods), mounted in the recording chamber, and the patch pipette was allowed to form a gigaseal. After measuring the basal calcium concentration of the cells in the on-cell configuration, the membrane patch was ruptured and the whole-cell configuration established. The internal solution was supplemented with 100 μM Fura-2 to assure the continued acquisition of Ca^{2+} signals in the whole-cell configuration. Upon break-in with 200 μM Sr^{2+} in the internal solution, Ca^{2+} levels increased to ~300 nM from resting levels of ~50 nM (Fig. 7 E). The cytosolic Ca^{2+} signal was composed of two components: a transient increase that was superimposed on a slower background increase, that reached a plateau after ~100 s. This apparent secondary signal is likely a Sr^{2+}-induced effect on Fura-2 fluorescence rather than a genuine

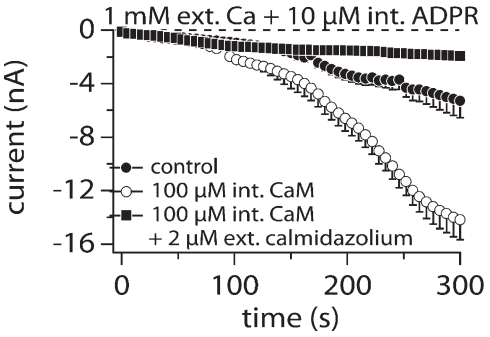

Figure 8. Calmodulin mediates facilitation of ADPR-induced TRPM2. Average inward TRPM2 currents evoked by 10 μM intracellular ADPR in the absence of exogenous buffers (closed circles, $n = 16$) and supplemented with 100 μM calmodulin in the presence (closed squares, $n = 4$) or absence (open circles, $n = 17$) of extracellular calmidazolium (2 μM). Standard extracellular saline contained 1 mM Ca^{2+}. Currents measured and analyzed as in Fig. 1. Error bars indicate SEM.

increase in Ca^{2+} concentration, since pretreatment with thapsigargin abolished the early Ca^{2+} transient but not the background signal. The Sr^{2+}-induced Ca^{2+} release signal can then be obtained by subtracting the calcium signal with thapsigargin incubation from the Ca^{2+} signal of the cells without thapsigargin incubation (Fig. 7 F). These experiments clearly show that Sr^{2+}-induced facilitation of TRPM2 activation occurs through an indirect mechanism, where external Sr^{2+} entering the cytosol releases Ca^{2+} from internal stores, which subsequently facilitates ADPR-induced TRPM2 activation.

Calmodulin Confers Ca^{2+}-mediated Facilitation of ADPR-induced TRPM2 Activation

The strong dependence of TRPM2 on $[Ca^{2+}]_i$ suggests the presence of a Ca^{2+} binding site on the channel or a Ca^{2+} sensor near the channel structure. One of the most plausible mechanisms for the latter seems to be calmodulin (CaM). It has been reported that CaM is an important requirement for TRPM2 activation (Tong et al., 2006). The authors suggested that Ca^{2+} influx through the TRPM2 channel enhances interaction of CaM with TRPM2 at the IQ-like motif in the N terminus, thus providing positive feedback for channel activation. Fig. 8 illustrates how this Ca^{2+} dependence is linked to CaM. The control data illustrates TRPM2 activation by 10 μM ADPR, a concentration close to the EC_{50} value. Hence, activation is relatively slow and the activated current reaches ~6 nA, which is about half its maximum amplitude (Fig. 8, closed circles). When 100 μM CaM is added to the internal solution (Fig. 8, open circles), activation becomes more rapid and the maximum current amplitude doubles, indicating that more channels are being activated. One of the possible explanations for this result is that the additional CaM near the TRPM2 channel has increased the sensitivity toward Ca^{2+}. To counteract this increased sensitivity to Ca^{2+}, we added 2 μM calmidazolium, a known CaM antagonist, to the extracellular medium. Under these conditions TRPM2 activation was strongly suppressed even in the presence of 100 μM CaM and 10 μM ADPR (Fig. 8, closed squares). We conclude that the facilitatory effect of Ca^{2+} on ADPR-induced TRPM2 activation is at least partially conferred by CaM.

DISCUSSION

The present study provides an encompassing assessment of the functional role of extra- and intracellular Ca^{2+} in regulating TRPM2 channel activity under close to physiological experimental conditions. Our results indicate that TRPM2 is affected by Ca^{2+} ions on both sides of the membrane. The channel can be gated in the complete absence of Ca^{2+} on either side, but is refractory when removing it on both sides. This indicates that Ca^{2+} is required and permissive for channel gating by ADPR, possibly requiring occupancy of a Ca^{2+} binding site within the channel pore that is accessible to Ca^{2+} from either side of the membrane. Although extracellular Ca^{2+} enables TRPM2 activation in the absence of intracellular Ca^{2+}, it does so without modulating Ca^{2+} sensitivity of the channel. Conversely, although intracellular Ca^{2+} is not required for channel gating, it greatly sensitizes TRPM2 to ADPR. This cytosolic effect of Ca^{2+} is mediated at least in part by calmodulin and synergizes with ADPR in channel activation. However, we also demonstrate that physiological, receptor-mediated Ca^{2+} release from intracellular stores in HEK293 cannot activate TRPM2 by itself, indicating that resting levels of ADPR in these cells are below the threshold for synergizing with Ca^{2+}.

Few previous studies explored the role of Ca^{2+} in the activation of TRPM2. An early report on a nonselective current in CRI-G1 insulinoma cells that was activated by NAD and H_2O_2 and was named NS_{NAD} (Herson et al., 1997) demonstrated the immediate closure of NAD-evoked single channels in the absence of intracellular Ca^{2+}. This current was later identified as TRPM2 (Inamura et al., 2003) and the ability of NAD to open TRPM2 channels is now thought to be caused by ADPR contamination of NAD rather than NAD itself (Kolisek et al., 2005). In CRI-G1 cells, the Ca^{2+} sensitivity of NS_{NAD} was measured in inside-out patches under high Na^+ conditions showing reduced open probability of these channels at negative potentials (Herson et al., 1997). Our own studies determined that intracellular Na^+ alters inactivation properties of TRPM2 whole-cell and single-channel currents in a voltage-dependent manner (Perraud et al., 2001). Further reports observed facilitation of ADPR-induced TRPM2 currents by Ca^{2+} in the HEK293 overexpression system (Perraud et al., 2001; Hara et al., 2002; McHugh et al., 2003), U937 monocytes

(Perraud et al., 2001), neutrophil granulocytes (Heiner et al., 2006), and CRI-G1 cells (Herson et al., 1997; Inamura et al., 2003). Interestingly, all of these studies were conducted using Cs^+-based intracellular solutions, which recently were found to alter the sensitivity of TRPM2 to ADPR (Beck et al., 2006). In addition, Na^+ can cause voltage-dependent inactivation of the channel (Perraud et al., 2001; Sano et al., 2001; Hara et al., 2002; McHugh et al., 2003).

TRPM2 has been reported to conduct Ca^{2+} in addition to monovalent ions (Perraud et al., 2001; Sano et al., 2001; Hara et al., 2002; McHugh et al., 2003). Our data show that Ca^{2+} conductance also occurs in the complete absence of Na^+ (Fig. 2). Curiously, TRPM2 currents start to oscillate under conditions where Ca^{2+} is further reduced to nominally Ca^{2+}-free levels. Combined Fura-2 and patch-clamp experiments show that this is caused by intracellular calcium oscillations, which occur independently of the presence of ADPR (Fig. 3 E). Such Ca^{2+} oscillations caused by absence of extracellular Na^+ and Ca^{2+} have been observed previously in CHO cells using tetramethylammonium (Ruth et al., 1993), although the causality of this phenomenon is currently not understood. Nevertheless, the Ca^{2+} oscillations explain the oscillatory behavior of TRPM2 under these experimental conditions and this interpretation is further corroborated by the observation that oscillatory behavior of TRPM2 currents is abolished when emptying the Ca^{2+} stores with the SERCA pump inhibitor thapsigargin. In addition, any manipulation that leads to increase in intracellular Ca^{2+}, such as exposure to thapsigargin, intracellular perfusion with IP_3, or stimulation with ionomycin, will enhance ADPR-induced TRPM2 behavior (Fig. 4). These data emphasize that the efficacy of TRPM2 activation is directly related to intracellular Ca^{2+} levels in the presence of sufficient ADPR.

The concentration-dependent activation of TRPM2 by ADPR yields EC_{50} values in the range of 10 to 200 μM, depending on intracellular Ca^{2+} levels (Fig. 5 A). This represents a significant dynamic range of ADPR-dependent TRPM2 activation, with threshold levels ranging between 5 and 100 μM ADPR. In neutrophil granulocytes, basal ADPR levels have been reported to be around 5 μM (Heiner et al., 2006). If this were so, basal ADPR levels would be high enough to cause TRPM2 activation simply by raising intracellular Ca^{2+} levels. However, in the HEK293 overexpression system, 5 μM ADPR already slightly activates TRPM2. This high sensitivity could result from the presence of intracellular Cs^+, which has been reported to facilitate ADPR-induced gating compared with K^+ conditions (Kolisek et al., 2005). This can be confirmed when comparing the EC_{50} for ADPR of 90 μM when using intracellular Cs^+ (Perraud et al., 2001) with the EC_{50} value of 200 μM we observe in K^+-based saline under otherwise identical conditions (Fig. 5 A). Furthermore, unlike in neutrophils, raising Ca^{2+} alone does not activate TRPM2 in intact HEK293 cells, as shown in our perforated patch experiment. Activation only occurs when exogenous ADPR is supplied above threshold via the patch pipette (see Fig. 3 F and Kolisek et al., 2005) and indicates that ADPR levels are <5 μM in HEK293 cells.

Since Cs^+ influences ADPR-induced gating, we wondered whether the modulation of TRPM2 gating by Ca^{2+} would also be affected. McHugh et al. (2003) completed a Ca^{2+} dose–response curve at fixed ADPR levels (500 μM) in overexpressed TRPM2 cells using intracellular Cs^+. Here, the apparent EC_{50} for Ca^{2+} was 340 nM, which is significantly less sensitive than the EC_{50} of 50 nM we see when using the same cell system but intracellular K^+ saline (Fig. 5 C). Hence, Ca^{2+} facilitation of ADPR-induced TRPM2 is at least sevenfold more sensitive in K^+ conditions. Furthermore, the observed Ca^{2+} effect on ADPR gating is solely conferred by internal Ca^{2+} since the absence of extracellular Ca^{2+} does not affect its EC_{50} (34 nM, Fig. 5 C). Thus, it appears that Cs^+ decreases ADPR sensitivity of TRPM2 at fixed Ca^{2+} levels, but enhances Ca^{2+}-dependent facilitation of the channel at fixed ADPR levels.

Interestingly, the complete absence of Ca^{2+} on both sides of the plasma membrane abolished TRPM2 activation by ADPR (Fig. 5 B and Fig. 6 A). This could be due to the prominent inactivation process seen when intracellular Ca^{2+} concentrations fall below 300 nM (Fig. 5 B), preventing ion flux through the channel. However, the extent of current inactivation is not significantly affected upon removal of extracellular calcium (Fig. 6, A and B). It is therefore unlikely that the inactivation process is responsible for suppressing current activation in the absence of Ca^{2+}. Rather, one has to consider the possibility of an extracellular Ca^{2+} binding site or a site within the pore of TRPM2 that is accessible to extracellular Ca^{2+}, and that needs to be occupied for proper channel function, especially when internal Ca^{2+} falls below 100 nM. Indeed, removal of extracellular Ca^{2+} after full activation of TRPM2 completely and irreversibly abolishes channel activity (Fig. 6 D). Thus, in the absence of intracellular Ca^{2+}, extracellular Ca^{2+} is mandatory for proper channel function. This channel behavior is similar, at least phenomenologically, to the behavior of CRAC (calcium release–activated calcium) channels, which undergo prominent depotentiation when exposed to divalent-free solutions (Hoth and Penner, 1993).

McHugh et al. (2003) proposed that effects of extracellular Ca^{2+} are due to Ca^{2+} influx and insufficient exogenous buffer capacity around the inner mouth of the channel rather than an extracellular binding site. This was based on the observation that the residual activation of TRPM2 currents observed at 100 nM fixed Ca^{2+} levels, even in the presence of high BAPTA concentrations (40 mM), could be prevented with a mixture of high and low affinity buffers. Our data indicate that

while 0 internal Ca^{2+} requires 1 mM extracellular Ca^{2+} to fully activate TRPM2, only 200 μM external Ca^{2+} is necessary when internal Ca^{2+} is minimally raised to 30 nM. However, 200 μM Ca^{2+} is unlikely to cause any significant Ca^{2+} influx to overpower exogenous buffers. This notion is further supported by the dose–response behavior of TRPM2 to $[Ca^{2+}]_i$, which is essentially independent of extracellular Ca^{2+} concentration.

The above data indicate that Ca^{2+} plays a pivotal role in TRPM2 function. The question arises of whether other divalent ions can substitute for Ca^{2+}. Two studies reported that Ba^{2+} cannot substitute for Ca^{2+} in activating single NS_{NAD} channels by NAD (or more likely contaminating ADPR) (Herson et al., 1997) or heterologously expressed TRPM2 (McHugh et al., 2003). Our data show that neither 10 mM Mg^{2+} nor Ba^{2+} affect the gating or change the activation kinetics of TRPM2 compared with nominally Ca^{2+}-free conditions (Fig. 7 A), confirming that these ions do not substitute for Ca^{2+}. Furthermore, extracellular Zn^{2+} inhibits TRPM2 completely. Interestingly, 10 mM Sr^{2+} showed comparable current sizes and current kinetics as seen with Ca^{2+}. However, this was due to Sr^{2+} causing Ca^{2+} release rather than the divalent binding to TRPM2 itself, further corroborating the importance of the facilitatory action of Ca^{2+} on ADPR-induced TRPM2 activation. Sr^{2+}-induced Ca^{2+} release has been observed in muscle contraction (Cognard and Raymond, 1985; Goblet and Mounier, 1987) and unicellular organisms (Bauer et al., 1998). Sr^{2+} is thought to interact with the ryanodine receptor, causing Ca^{2+} release. Since HEK293 cells have been reported to respond to caffeine treatment with Ca^{2+} release (Luo et al., 2005), this may be the underlying mechanism or a contributing factor for the observed effect.

The question remains of whether intracellular Ca^{2+} interacts directly with TRPM2 or via a Ca^{2+}-sensitive modulator. Calmodulin is a ubiquitously expressed protein involved in the calcium-dependent regulation of proteins, including activation and inactivation processes of plasma membrane and intracellular channels (Saimi and Kung, 2002). Calmodulin binding to TRPM2's N terminus has been implicated to confer the channel's Ca^{2+} sensitivity (Tong et al., 2006). This was demonstrated using Mn^{2+} quenching of FuraRed in intact cells while cooverexpressing various calmodulin mutants. In the present study, we demonstrate that direct supply of CaM to the cytosol via the patch pipette in the presence of only 10 μM ADPR indeed significantly facilitates ADPR-induced TRPM2 activation. In support of this notion, the addition of calmidazolium, an inhibitor of calmodulin, to the bath medium almost completely suppresses TRPM2 activation under the same experimental conditions. This strongly indicates that Ca^{2+}-bound calmodulin interacts with TRPM2 and is largely responsible for facilitating ADPR-induced channel activity. Furthermore, the CaM-mediated regulation may be accountable for the inactivation of TRPM2 observed at low $[Ca^{2+}]_i$, since less CaM is in the Ca^{2+}-bound form and diffusional escape of CaM into the patch pipette during whole-cell perfusion further reduces the CaM available for facilitation of the channels.

In conclusion, our data provide evidence that ADPR and Ca^{2+} are synergistic cofactors in regulating TRPM2 activity. While ADPR is a required agonist that gates TRPM2 in a dose-dependent manner in the absence of intracellular Ca^{2+}, Ca^{2+} itself is not able to recruit TRPM2 at any reasonable physiological concentration but facilitates ADPR-dependent activation. Physiologically, this situation would suggest that ADPR acts as a switch to enable TRPM2 gating, whereas intracellular Ca^{2+} levels in the physiological range of ∼50 nM to ∼1 μM modulates the sensitivity of TRPM2 to ADPR. This effect of intracellular Ca^{2+} is likely mediated by calmodulin. However, even under optimal Ca^{2+} conditions, the EC_{50} for ADPR does not fall below 10 μM in the absence of further modulatory mechanisms such as, e.g., cADPR (Kolisek et al., 2005). Interestingly, $[Ca^{2+}]_i$ not only facilitates ADPR-induced activation of TRPM2 but is required for sustained channel activity, since low $[Ca^{2+}]_i$ results in channel inactivation. In the most extreme case, removal of Ca^{2+} from either side of the membrane completely suppresses any TRPM2 activity. This block can be overcome by admitting Ca^{2+} to any side of the membrane, suggesting a Ca^{2+} binding site on TRPM2 that is accessible from either side of the membrane and must be occupied by Ca^{2+} for proper channel function. Thus, TRPM2 is under regulatory control of a multitude of cytosolic factors that all appear to synergize on channel activation.

We thank Miyoko Bellinger for excellent technical support.

This work was supported by Hawaii Community Foundation grant 20061480 (J. Starkus), Queen Emma Research Foundation grant PA-2006-040 (A. Beck), and National Institutes of Health grant R01-GM063954 (R. Penner).

Olaf S. Andersen served as editor.

Submitted: 5 June 2007
Accepted: 7 September 2007

REFERENCES

Bauer, C.S., C. Plieth, B. Bethmann, O. Popescu, U.P. Hansen, W. Simonis, and G. Schonknecht. 1998. Strontium-induced repetitive calcium spikes in a unicellular green alga. *Plant Physiol.* 117:545–557.

Beck, A., M. Kolisek, L.A. Bagley, A. Fleig, and R. Penner. 2006. Nicotinic acid adenine dinucleotide phosphate and cyclic ADP-ribose regulate TRPM2 channels in T lymphocytes. *FASEB J.* 20:962–964.

Cognard, C., and G. Raymond. 1985. The strontium-induced calcium-release process and its implication in contractility of skeletal muscle of *Rana ridibunda*. *Proc. R. Soc. Lond. B. Biol. Sci.* 224:489–509.

Fleig, A., and R. Penner. 2004. The TRPM ion channel subfamily: molecular, biophysical and functional features. *Trends Pharmacol. Sci.* 25:633–639.

Goblet, C., and Y. Mounier. 1987. Activation of skinned muscle fibers by calcium and strontium ions. *Can. J. Physiol. Pharmacol.* 65:642–647.

Hara, Y., M. Wakamori, M. Ishii, E. Maeno, M. Nishida, T. Yoshida, H. Yamada, S. Shimizu, E. Mori, J. Kudoh, et al. 2002. LTRPC2 Ca^{2+}-permeable channel activated by changes in redox status confers susceptibility to cell death. *Mol. Cell.* 9:163–173.

Harteneck, C. 2005. Function and pharmacology of TRPM cation channels. *Naunyn Schmiedebergs Arch. Pharmacol.* 371:307–314.

Heiner, I., J. Eisfeld, M. Warnstedt, N. Radukina, E. Jungling, and A. Luckhoff. 2006. Endogenous ADP-ribose enables calcium-regulated cation currents through TRPM2 channels in neutrophil granulocytes. *Biochem. J.* 398:225–232.

Herson, P.S., and M.L. Ashford. 1997. Activation of a novel nonselective cation channel by alloxan and H2O2 in the rat insulin-secreting cell line CRI-G1. *J. Physiol.* 501(Pt 1):59–66.

Herson, P.S., K.A. Dulock, and M.L. Ashford. 1997. Characterization of a nicotinamide-adenine dinucleotide-dependent cation channel in the CRI-G1 rat insulinoma cell line. *J. Physiol.* 505(Pt 1): 65–76.

Hoth, M., and R. Penner. 1993. Calcium release-activated calcium current in rat mast cells. *J. Physiol.* 465:359–386.

Inamura, K., Y. Sano, S. Mochizuki, H. Yokoi, A. Miyake, K. Nozawa, C. Kitada, H. Matsushime, and K. Furuichi. 2003. Response to ADP-ribose by activation of TRPM2 in the CRI-G1 insulinoma cell line. *J. Membr. Biol.* 191:201–207.

Kolisek, M., A. Beck, A. Fleig, and R. Penner. 2005. Cyclic ADP-ribose and hydrogen peroxide synergize with ADP-ribose in the activation of TRPM2 channels. *Mol. Cell.* 18:61–69.

Launay, P., A. Fleig, A.L. Perraud, A.M. Scharenberg, R. Penner, and J.P. Kinet. 2002. TRPM4 is a Ca^{2+}-activated nonselective cation channel mediating cell membrane depolarization. *Cell.* 109:397–407.

Luo, D., H. Sun, R.P. Xiao, and Q. Han. 2005. Caffeine induced Ca^{2+} release and capacitative Ca^{2+} entry in human embryonic kidney (HEK293) cells. *Eur. J. Pharmacol.* 509:109–115.

McHugh, D., R. Flemming, S.Z. Xu, A.L. Perraud, and D.J. Beech. 2003. Critical intracellular Ca^{2+} dependence of transient receptor potential melastatin 2 (TRPM2) cation channel activation. *J. Biol. Chem.* 278:11002–11006.

Perraud, A.L., A. Fleig, C.A. Dunn, L.A. Bagley, P. Launay, C. Schmitz, A.J. Stokes, Q. Zhu, M.J. Bessman, R. Penner, et al. 2001. ADP-ribose gating of the calcium-permeable LTRPC2 channel revealed by Nudix motif homology. *Nature.* 411:595–599.

Ruth, P., G.X. Wang, I. Boekhoff, B. May, A. Pfeifer, R. Penner, M. Korth, H. Breer, and F. Hofmann. 1993. Transfected cGMP-dependent protein kinase suppresses calcium transients by inhibition of inositol 1,4,5-trisphosphate production. *Proc. Natl. Acad. Sci. USA.* 90:2623–2627.

Saimi, Y., and C. Kung. 2002. Calmodulin as an ion channel subunit. *Annu. Rev. Physiol.* 64:289–311.

Sano, Y., K. Inamura, A. Miyake, S. Mochizuki, H. Yokoi, H. Matsushime, and K. Furuichi. 2001. Immunocyte Ca^{2+} influx system mediated by LTRPC2. *Science.* 293:1327–1330.

Scharenberg, A.M. 2005. TRPM2 and TRPM7: channel/enzyme fusions to generate novel intracellular sensors. *Pflugers Arch.* 451:220–227.

Tong, Q., W. Zhang, K. Conrad, K. Mostoller, J.Y. Cheung, B.Z. Peterson, and B.A. Miller. 2006. Regulation of the transient receptor potential channel TRPM2 by the Ca^{2+} sensor calmodulin. *J. Biol. Chem.* 281:9076–9085.

Wehage, E., J. Eisfeld, I. Heiner, E. Jungling, C. Zitt, and A. Luckhoff. 2002. Activation of the cation channel long transient receptor potential channel 2 (LTRPC2) by hydrogen peroxide. A splice variant reveals a mode of activation independent of ADP-ribose. *J. Biol. Chem.* 277:23150–23156.